

rsta.royalsocietypublishing.org



CrossMark
click for updates

Research

Cite this article: McRobie A, Morgenthal G, Abrams D, Prendergast J. 2013 Parallels between wind and crowd loading of bridges. *Phil Trans R Soc A* 371: 20120430. <http://dx.doi.org/10.1098/rsta.2012.0430>

One contribution of 17 to a Theme Issue 'A celebration of mechanics: from nano to macro'

Subject Areas:

structural engineering

Keywords:

bridges, dynamics, wind, human–structure interaction, aeroelasticity

Author for correspondence:

Allan McRobie

e-mail: fam@eng.cam.ac.uk

Parallels between wind and crowd loading of bridges

Allan McRobie¹, Guido Morgenthal², Danny Abrams³ and John Prendergast⁴

¹Department of Engineering, University of Cambridge, Cambridge CB2 1PZ, UK

²Bauhaus-Universität Weimar, 99421 Weimar, Germany

³Department of Engineering Sciences and Applied Mathematics, Northwestern University, Evanston, IL 60208-3125, USA

⁴Renewable Energy Systems Ltd, Beaufort Court, Egg Farm Lane, Kings Langley WD4 8LR, UK

Parallels between the dynamic response of flexible bridges under the action of wind and under the forces induced by crowds allow each field to inform the other. Wind-induced behaviour has been traditionally classified into categories such as flutter, galloping, vortex-induced vibration and buffeting. However, computational advances such as the vortex particle method have led to a more general picture where effects may occur simultaneously and interact, such that the simple semantic demarcations break down. Similarly, the modelling of individual pedestrians has progressed the understanding of human–structure interaction, particularly for large-amplitude lateral oscillations under crowd loading. In this paper, guided by the interaction of flutter and vortex-induced vibration in wind engineering, a framework is presented, which allows various human–structure interaction effects to coexist and interact, thereby providing a possible synthesis of previously disparate experimental and theoretical results.

1. Introduction

This paper investigates the parallels between wind- and human-induced vibration phenomena on bridges. There is no attempt to argue by analogy, because that approach has no intellectual basis. Rather, by noting the parallels, the techniques and understandings developed in one field may inform the study of the other.

For pivotal moments, wind engineering had the collapse of the first Tacoma Narrows Bridge in the USA in 1940, and human-induced vibration had the openings of the Solférino (now Léopold-Sédar-Senghor) Bridge in Paris, France, in 1999 and the Millennium Bridge in London, UK, in 2000. These events defined their fields: the post-Tacoma research by Farquharson *et al.* [1] led on to the subsequent decades of progress in bridge aeroelasticity, and although large lateral responses of a crowded footbridge had been reported earlier [2], it was the experiments by Arup [3], with crowds on the Millennium Bridge, that led on to detailed quantification of human–structure interaction effects. Large lateral oscillations under crowd loading have been reported on many bridges before and since. A partial list is given in Venuti & Bruno [4] within a review of research up to 2009. An occurrence on the Bosphorus Bridge, Istanbul, in 2010 [5], provides further evidence that the phenomenon is not restricted to lightweight footbridges. More worryingly, the panic that resulted in 119 deaths on a crowded bridge in Cambodia in 2010 has been attributed to large lateral motions leading to a fear of incipient collapse [6].

Although walkers exert forces in all directions, the focus of this paper is on the *lateral* behaviour that has been the subject of greatest recent interest. Similarly, the focus for wind is on the *vertical and torsional* responses such as were observed at Tacoma. In each case, the paper considers the forces on a static structure before looking at how those forces evolve as a result of the bridge's dynamic response.

2. The basic forces on a static structure

The lateral forces exerted by a walker on a static surface are of approximately square-wave form with a frequency near 1 Hz [7]. In a first assessment, a designer might consider the response to the first harmonic of a single 'bad walker' to be indicative of the bridge's susceptibility to lateral problems, this having been the traditional approach to vertical effects.

The comparable wind-engineering effect is vortex shedding. Boundary layers develop along the deck surfaces, creating vorticity which is shed as shear layers that propagate downstream and roll up via a Kelvin–Helmholtz instability to form the familiar von Kármán vortex street, creating periodic crosswind forces that can excite the bridge into vertical or torsional responses.

These then are the basic forces—the lateral forces associated with each step and the vertical forces associated with each vortex. In the simplest case, each force is assumed to be harmonic, and it is assumed that the forces do not evolve in response to the bridge motion. This approach can be generalized while still assuming no feedback: in the human–structure case, the single 'bad walker' indicator can be replaced by a performance-based design approach by considering crowds with walking speeds, pacing frequencies, forcing magnitudes and phases selected randomly from appropriate distributions. Forward integration of a time-domain model can then predict the multi-modal response to the mode-generalized forces applied by the crowd [8,9], thereby indicating the likely vibration levels in a set of plausible scenarios, such as the passage of several joggers or a larger group of walkers.

The basic wind forces have two elements of randomness. One concerns incident turbulence, typically described via the spectral approach and the aerodynamic admittance of Davenport [10], the Engineering Science Data Unit [11], Lawson [12] and others. The second concerns the span-wise decorrelation of von Kármán vortices. The consequent reduction in the magnitude of the mode-generalized forces—compared with those obtained assuming full span-wise correlation—can be modelled by incorporating empirical estimates of correlation length into the spectral approach [13].

3. Frequency lock-in

That the structural response can feed back and affect the forcing is well known for vortex-induced vibrations [14]. Vortices are released differently from moving than from stationary surfaces such that the shedding frequency can lock in to the structural frequency. The susceptibility of a structural mode to such vortex-induced resonance is indicated by the Scruton number, a dimensionless mass-damping parameter. Modes with Scruton numbers below 15 are typically

problematic [13], but the response is generally self-limiting, with crosswind displacement amplitudes being roughly proportional to the reciprocal of the Scruton number. For chimneys, the problem can be substantially ameliorated by helical strakes that disrupt the span-wise correlation. For bridges, adjustments to the cross-section profile—such as the guide vanes fitted to the lower corners of the Storebælt Bridge in Denmark [15]—can influence the way that vorticity is released into the wake to advantageous effect.

For the human–structure case, an analogous ‘pedestrian Scruton number’ was proposed in McRobie & Morgenthal [16]. This was a mass-damping parameter with the dimensionless mass being a ratio of bridge to crowd mass (rather than bridge to air mass). It was proposed that structural modes with sufficiently high pedestrian Scruton number—achieved perhaps by provision of additional damping—could then be assumed to avoid the lateral instability under crowd loading, and that a survey of problematic and non-problematic bridges would reveal the pedestrian Scruton number levels required to avoid problems.

The lock-in concept was applied to the human–structure case in the Strogatz *et al.* [17] synchronization model: walkers creating lateral forces that were originally at randomized frequencies adjust their footfall timings to walk in phase synchrony with the bridge motions (and thus with each other). Such feedback was proposed as the mechanism underlying the instability of the lateral responses of bridges near 1 Hz. In this model, the bridge response begins small, the fluctuations of the basic randomized forces being initially insufficient to overcome the structural damping. However, as more people walk onto the bridge, the structural amplitudes begin to grow, and once a critical number of people is exceeded, the rate at which forces grow owing to more walkers becoming entrained to the bridge frequency exceeds the rate at which those forces can be overcome by structural damping. The result is a divergent oscillatory growth of vibrations.

4. Forces induced at the structural frequency

Building on an idea of Barker [18], Macdonald [19] models each walker as an inverted pendulum between successive foot placements, with foot placement strategies that provide stable long-term balance. The unobvious prediction of this model is that, even if the walker maintains a constant pacing frequency different from that of the bridge, there are force components created *at the bridge frequency* as a result of the modulation in foot placement offset relative to the deck. Some care is needed with terminology. Macdonald’s model leads to the prediction of forces synchronous with the bridge motion, but the walker does not synchronize the timings of their footsteps.

Macdonald’s model successfully describes the gaits observed for walkers on structures oscillating at low frequency, predicting how the walker’s centre of mass follows an undulating trajectory at the bridge frequency, with the footsteps pattering either side of that trajectory at their original higher-pacing frequency (figure 1). It follows from the centre of mass motions that there will be a force on the bridge at the bridge frequency. Some component of that force will be in phase with the bridge velocity and may feed energy into the bridge. Instability then occurs if these forces exceed the structural damping.

The appropriate measure of the force component in phase with the bridge velocity is the c_p value, this being the constant of proportionality between the induced force component f_v and the local velocity \dot{x} of the bridge (i.e. $f_v = c_p \dot{x}$). There is another, less important, component in phase with the bridge acceleration, $f_a = \rho_m m \ddot{x}$, with m the pedestrian’s mass and ρ_m the proportionality constant.

The fluid–structure parallel to these in-phase force components are the forcing terms associated with flutter. Classical flutter involves a torsional (pitch) and a vertical (heave) mode, coupled by motion-induced lift forces and moments. For symmetric sections, the equations take the form

$$\begin{aligned} \ddot{h} + 2\xi_h \omega_h \dot{h} + \omega_h^2 h &= \frac{L_h}{m} \\ \text{and} \quad \ddot{\theta} + 2\xi_\theta \omega_\theta \dot{\theta} + \omega_\theta^2 \theta &= \frac{M_\theta}{I} \end{aligned} \quad (4.1)$$

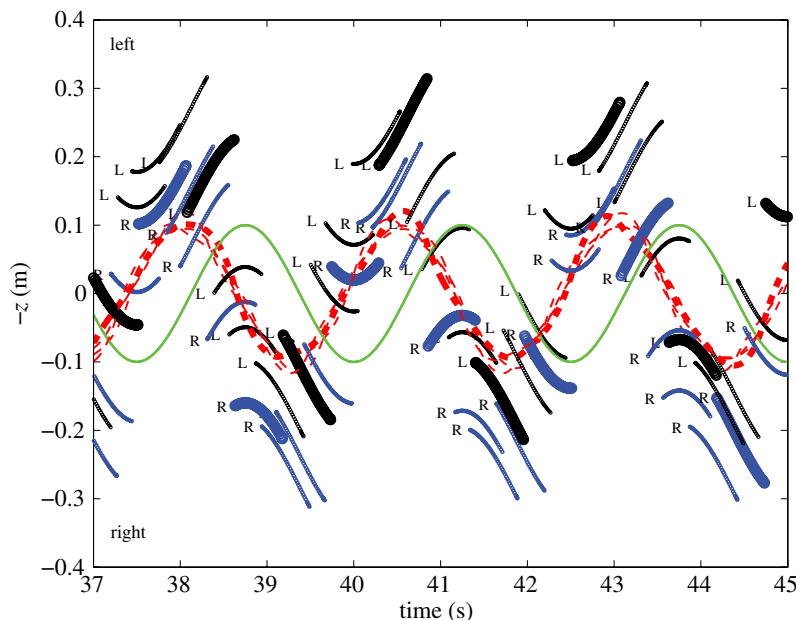


Figure 1. The predictions of Macdonald's model for the foot placements of four walkers at 0.9 Hz on a 0.4 Hz bridge. The walkers' centres of mass (central dashed near-sinusoids) can be seen to follow undulating paths at the bridge frequency (central solid sinusoid), even though the footfalls patter either side at their original frequency. The footfalls of one walker are emboldened. (Online version in colour.)

with h, θ the heave and pitch, and the appropriately subscripted ω and ξ being the corresponding undamped natural frequencies and fractions of critical damping, with m and I the mass and mass moment of inertia, each per unit length. The coupling occurs via the lift L_h and moment M_θ on the right-hand side. If it is assumed that the motion is harmonic, these may be linearized to

$$\begin{bmatrix} L_h \\ \frac{1}{2}\rho U^2 B \\ M_\theta \\ \frac{1}{2}\rho U^2 B^2 \end{bmatrix} = \begin{bmatrix} H_1^* & H_2^* & H_3^* & H_4^* \\ A_1^* & A_2^* & A_3^* & A_4^* \end{bmatrix} \begin{bmatrix} \frac{K\dot{h}}{U} \\ \frac{KB\dot{\theta}}{U} \\ K^2\theta \\ \frac{K^2 h}{B} \end{bmatrix}, \quad (4.2)$$

where ρ, U and B are the air density, incident wind velocity and cross-section chord length. The parameter $K = B\omega/U$ is the reduced frequency, a non-dimensional expression of the structural frequency ω . The reduced velocity v_r is defined as $2\pi/K$, a dimensionless measure of the incident wind speed.

For plate-like cross sections, Theodorsen theory [20] provides the relevant 'flutter derivatives'—the dimensionless frequency-dependent coefficients $H_i^*(K)$ and $A_i^*(K)$ that relate the motion amplitudes to the motion-induced forces. The wake is taken as a single (rather than double) shear layer and has a sinusoidal form as it trails downwind. Theodorsen's theory assumes that there is no Kelvin–Helmholtz instability—the trailing wake does not roll itself up further. The vorticity concentrated in this sinusoidal shear layer influences the new vorticity created back at the surfaces of the moving structure.

Theodorsen's approach was extended to bluff bodies by Scanlan & Tomko [21]. The equations are assumed to take the form of equation (4.2), but the coefficients for a particular cross section, rather than being computed, are measured across a range of prescribed frequencies on section

model tests in a wind tunnel. The procedure assumes that the cross section is sufficiently bluff that separation points will be determined by the profile corners such that there will be Reynolds number independence allowing transfer from laboratory to full scale.

The parallel between flutter and human–structure interaction is striking. In the human–structure case, the lateral force component induced at the bridge frequency is $f = c_p \dot{x} + \rho_m m \ddot{x}$ and, proportionality factors apart, the coefficients c_p and $\rho_m m$ are entirely analogous to the flutter derivatives [22] (there being an additional proportionality factor to convert the harmonic acceleration to the harmonic displacement). In both the wind- and human-induced cases the flutter derivatives are defined by linearization and are thus, theoretically at least, *independent of bridge amplitude*.

In what may be described as ‘pedestrian section model tests’, Ingólfsson *et al.* [23] measured such coefficients in a laboratory, putting single walkers on a treadmill on a moveable platform that could be put through prescribed harmonic displacements of differing amplitudes and frequencies. The approach is entirely analogous to the wind-tunnel section model tests of Scanlan’s procedure. However, it is questionable whether laboratory results can be transferred to full scale for humans as readily as can be done for wind. For example, parallax clues from adjacent objects in the laboratory will have psychological effects that may affect the foot placement control law, walking on a treadmill at constant speed gives fewer options for adjustment of walking speed and foot placement, and walking alone can be very different from walking in a crowd where there may be oncoming pedestrians to be avoided and where there may be many subtle psychological influences arising from the presence of walkers adjacent and in front. Noting that the Ingólfsson *et al.* [23] measurements for c_p were less than—and often considerably less than—the values measured by Arup [3], it may be prudent for designers to use the latter, higher values, because these were derived from experiments conducted with crowds on a full-scale bridge.

There is a similar mismatch between the ‘pedestrian flutter derivatives’ predicted by Macdonald’s model and the Arup result of $c_p = 300 \text{ N s m}^{-1}$ over the full 0.5–1 Hz frequency range. Macdonald presented two possibilities for the foot placement control law, with placement choice dependent either on the absolute velocity of the walker’s centre of mass or on its velocity relative to the bridge deck. For the absolute velocity control law, the model predicts $c_p \approx 220 \text{ N s m}^{-1}$ near 0.5 Hz, not too far from the Arup measurements. However, near 1 Hz, the Macdonald model predicts $c_p \approx 140 \text{ N s m}^{-1}$ independent of control law. This is less than half the value measured by Arup. Extending the set of possible control laws—making foot placement more generally dependent upon bridge motions—can lead to gaits capable of creating larger c_p in the 1 Hz region. Alternatively, larger c_p values might arise if some of the walkers were to synchronize their footsteps with the bridge motion, as described by Strogatz *et al.* [17], and the possibility of such interaction is explored in a later section.

5. Two-dimensional section modelling

The parallel between fluid- and human–structure interaction is perhaps best illustrated by a comparison of figures 1 and 2. Both correspond to prescribed harmonic motions of the bridge deck at a frequency lower than human pacing or von Kármán shedding, respectively. The former shows the foot placements according to Macdonald’s model, with the feet pattering rapidly either side of the low-frequency undulations of the walker’s centre of mass. Figure 2, by comparison, shows the vorticity generated by the oscillating bluff bridge deck with the long-wavelength, low-frequency sinusoidal sweep of the Theodorsen-like flutter wake extending from left to right across the figure, adorned by higher frequency von Kármán vortices that are shed from alternate sides of the structure.

In each case, there are phenomena at two different frequencies: the high-frequency basic forces (at the walker’s pacing frequency and from the von Kármán street) and the lower-frequency motion-induced forces (from the sinusoidal undulations of the walker’s centre of mass and from the Theodorsen-like flutter wake). The question naturally arises as to whether

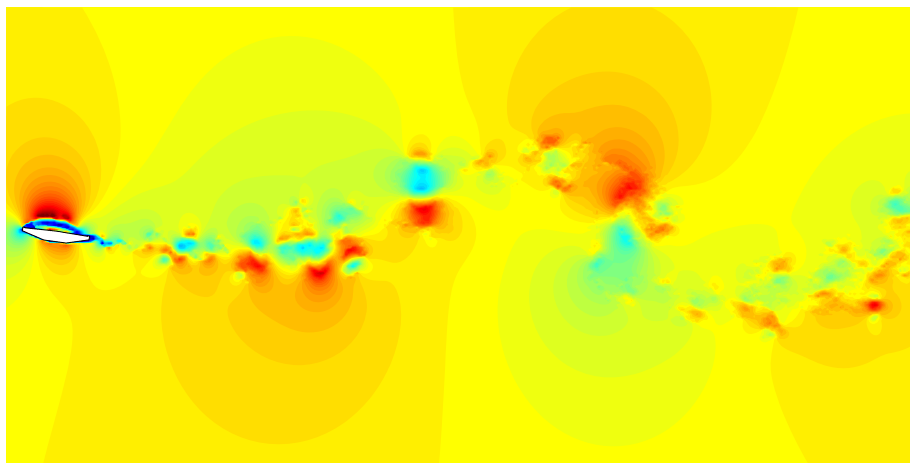


Figure 2. The wake behind an oscillating section of the Millau Viaduct, France. Long-wavelength sinusoidal undulations associated with the low-frequency bridge motions are adorned on either side by von Kármán vortices being shed at higher frequencies from the upper and lower deck corners and surfaces. The figure was produced using Morgenthal's VXFLOW [24]. (Online version in colour.)

the phenomena at the different frequencies can interact if the wavelength of the flutter wake becomes comparable to the von Kármán spacing or if the pacing frequency is close to that of the bridge.

(a) Flutter–vortex-induced vibration interaction

For bridge sections, von Kármán shedding and flutter are usually treated separately, because each tends to dominate at a particular wind speed—low speeds for vortex-induced vibration and high speeds for flutter. There are cases, however, when such easy demarcation is not possible.

Experimental evidence for flutter–vortex-induced vibration interaction may be found in Deniz & Staubli [25,26]. In particular, fig. 5a of [26] shows the lift curves for an elongated and tilted rectangular section subject to prescribed harmonic crosswind displacements. The basic feature is an amplitude-independent flutter curve garlanded by amplitude-dependent curves in the region where vortex shedding and flutter frequencies are comparable. van der Pol-type models have been proposed to generate the amplitude-limited limit cycle at lock-in [27], and such nonlinear terms can be incorporated into a flutter derivative formulation to arrive at a model capable of flutter–vortex-induced vibration interaction [28]. Scanlan [29] presented an alternative description of flutter–vortex-induced vibration interaction which, like the basic flutter derivative formulation for bluff bodies, provides a way of extrapolating wind tunnel results to full scale.

Before its collapse, the Tacoma Narrows Bridge underwent a variety of large-amplitude responses, including a purely vertical motion before the predominantly torsional response which led to its destruction. Billah & Scanlan [30] describe how many physics textbooks erroneously explain the collapse as an example of ‘resonance’. The explanation that has since gained general acceptance in the wind-engineering community is that it was single-degree-of-freedom torsional flutter, which can arise when the A_2^* derivative changes sign and the motion-induced forces overcome the small structural damping of the torsional mode.

It was only with Larsen's analysis [31] using the vortex particle (or discrete vortex) method that a physics-based explanation of the collapse was finally presented. Larsen's detailed and highly visual modelling of the fluid revealed how large vortices were created by the leading edges of the oscillating structure and were then convected along the deck (figure 3). These vortices were generated alternately at the upper and lower leading edges, and released in synchrony



Figure 3. A vortex particle simulation of the first Tacoma Narrows Bridge undergoing large-amplitude prescribed periodic torsional motions. The figure, produced using Morgenthal's VXFLOW [24], illustrates Larsen's vortex drift hypothesis, with large leading-edge vortices drifting across the deck, above and below, inducing periodic forces on the leeward portions of the deck.

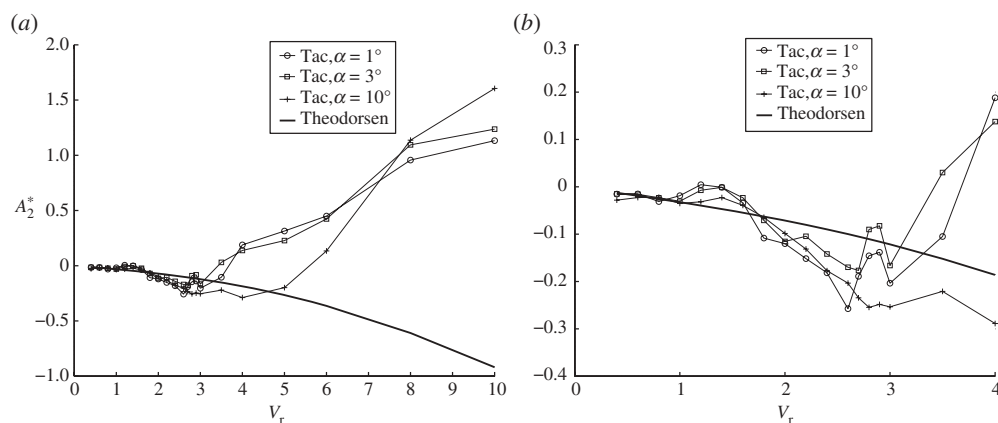


Figure 4. (a) The flutter derivative A_2^* for a Tacoma-like H-section (calculated using Morgenthal's VXFLOW [24]). (b) A zoom at low reduced velocity.

with—and as a consequence of—the large-amplitude bridge motions. The pressure distribution around the deck (and thus the associated forces) can be calculated precisely within the vortex particle framework, allowing flutter derivatives to be calculated. Figure 4 shows the A_2^* derivative so determined by Morgenthal's VXFLOW [24] for a Tacoma-like H-section. For plate-like sections, Theodorsen theory predicts that A_2^* is always negative, corresponding to positive aerodynamic damping. However for a bluff section, A_2^* can become positive (corresponding to negative aerodynamic damping), and should this exceed the structural damping, then oscillatory torsional divergence will result.

The Strouhal number computed by VXFLOW for the static Tacoma section, measured in the far wake, corresponds to a reduced velocity of around 1.4, giving a first indication of where flutter and vortex lock-in might be expected to interact once structural motions begin. The computed A_2^* derivative (figure 4) does indeed exhibit some amplitude dependence in this region, becoming zero for small-amplitude vibrations. However, while this is consistent with the simplest view of flutter–vortex-induced vibration interaction, it does not explain the Tacoma collapse, because the catastrophic divergent oscillations correspond to the more dramatic change of sign of A_2^* that occurs at reduced velocities above 3.

The large vortices produced at the leading (rather than trailing) vertical edges are key to understanding the collapse, and Larsen [31] describes the phasing of the local moments generated as each vortex passes across the deck. This is Larsen's 'vortex drift hypothesis': that at a reduced velocity of around twice that of the Strouhal resonance the drifting vortices above and below the deck do no net torsional work on the deck, and at reduced velocities above this, net work is

done and divergent oscillations begin. Whether such oscillations are described as vortex induced, flutter or galloping is somewhat irrelevant. With its focus on the underlying physics, the vortex particle method transcends the problematics of verbal categorization. Vorticity is created at the fluid–structure interfaces and convected in obedience of the Biot–Savart law and the Kelvin circulation theorems. The structure responds to the resulting pressures, and the resulting motions influence the vorticity creation. It is inappropriate to categorize this complexity as vortex-induced resonance or flutter, for it is neither, both and more.

6. Interaction in the human–structure case

Against this backdrop the possibility of a more complete model for human–structure interaction is now considered. There are two disparate theories: the Macdonald model that holds walking frequency constant but has variable (and non-harmonic) forcing amplitude, and the Strogatz synchronization theory that holds the forcing amplitude constant but allows the walking frequency and phase to evolve. The synthesis proposed here takes Macdonald’s biomechanically based inverted pendulum model, but relaxes the requirement of fixed walking frequency, thereby allowing some walkers to synchronize their footfalls with bridge motions. One reason for proposing such a synthesis stems from the disparities that exist between the differing experimental results of Arup [3] and of Ingólfsson *et al.* [23] and the differing predictions of the two theoretical models.

For walkers just away from perfect tuning with a bridge motion near 1 Hz, the Macdonald model predicts quasi-periodic solutions. As bridge amplitudes build, these gaits require the walker to walk for prolonged periods with their feet crossed. While walkers have been observed to cross their feet when walking on a moving surface, it may be hypothesized that others will adjust their gait—particularly if there is a sense of danger of possible loss of balance—to a more normal, more comfortable gait with widely spaced uncrossed feet.

The Macdonald model’s prediction of $c_p \approx 140 \text{ N s m}^{-1}$ at perfect tuning near 1 Hz irrespective of control law masks the fact that this is an average over all relative phases. At general frequencies, walkers cycle quasi-periodically through all possible relative phases, giving a single long-time average c_p value. However, at perfect tuning, there is no quasi-periodicity to average over, and the c_p generated depends on the relative phase between walker and bridge. For a 0.86 Hz walker, the variation of c_p with bridge frequency is shown in figure 5*a*, together with a synopsis of various experimental results. The corresponding variation of c_p with phase at perfect tuning is given in figure 5*b*, showing that Macdonald’s model contains solutions at perfect tuning that can provide c_p values higher than the circa 140 N s m^{-1} phase-averaged value. The hypothesis of this paper is that some walkers may tune to the bridge frequency and selectively adopt these higher c_p gaits.

Figure 6*a* shows absolute foot placements for a walker whose pacing frequency is marginally detuned from that of the bridge. Figure 6*b* shows the corresponding trajectories of a suitably chosen variable S within the Macdonald model. S is the complexified version of $s = y + \dot{y}/\Omega + (C_0 + 1)x + C_1\dot{x}/\Omega$, where x is the bridge displacement, y is the displacement of the walker’s centre of mass relative to the bridge, and C_0, C_1 are coefficients in the foot placement control law (taken here as $C_0 = 0$ and $C_1 = 1$, corresponding to the absolute velocity control law). The reason for the choice of s is that it is continuous and quasi-periodic *ab initio*, requiring no transient burn-in. Moreover, at the instant a foot is placed, $s = z_0 \mp b$, where z_0 is the absolute foot placement, such that the absolute foot placement can be discerned (up to $\pm b$) from the diagram. A Poincaré section of the flow sampling S at each right foot placement shows that the Macdonald model contains an underlying circle map—this being the set of points on the right large circle. Given the existence of such a map, a natural construction for a synchronization model would be to make minor adjustments to the pacing period such that the quasi-periodic trajectory converges to a period-1 fixed point on a nearby circle map.

Such a model can be obtained by discretizing the continuous Strogatz *et al.* [17] equation for the evolution of the phase Θ of the force exerted by a walker,

$$\dot{\Theta} = \omega_w + CX_{br} \sin(\Psi - \Theta + \alpha), \quad (6.1)$$

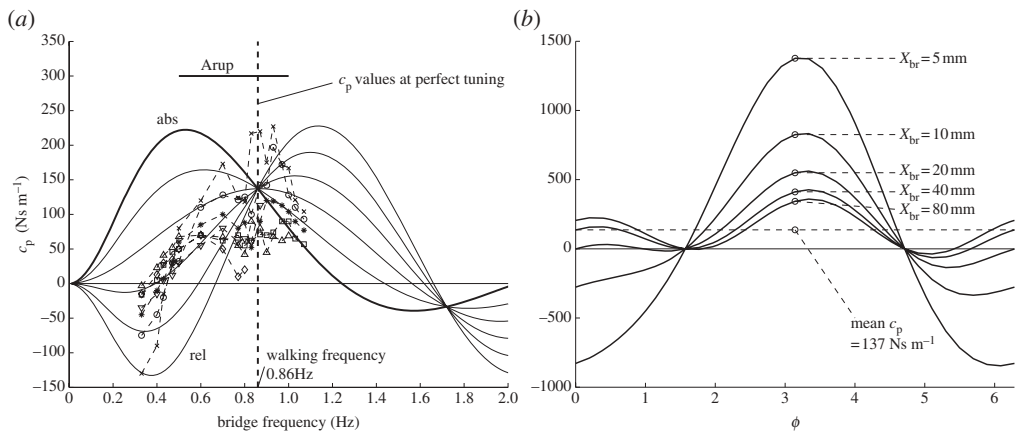


Figure 5. The c_p curves of the Macdonald model, for a 74.4 kg walker at 0.86 Hz (other parameters as per Macdonald [19]). (a) The variation of c_p with bridge frequency, for both absolute and relative velocity control laws (and four variants between these). The experimental results of Arup [3] and Ingólfsson *et al.* [23] are superposed (albeit that the walkers in the latter had walking frequencies distributed around 0.86 Hz). (b) The displacement-dependent variation of c_p with phase at perfect tuning (for the absolute velocity control law).

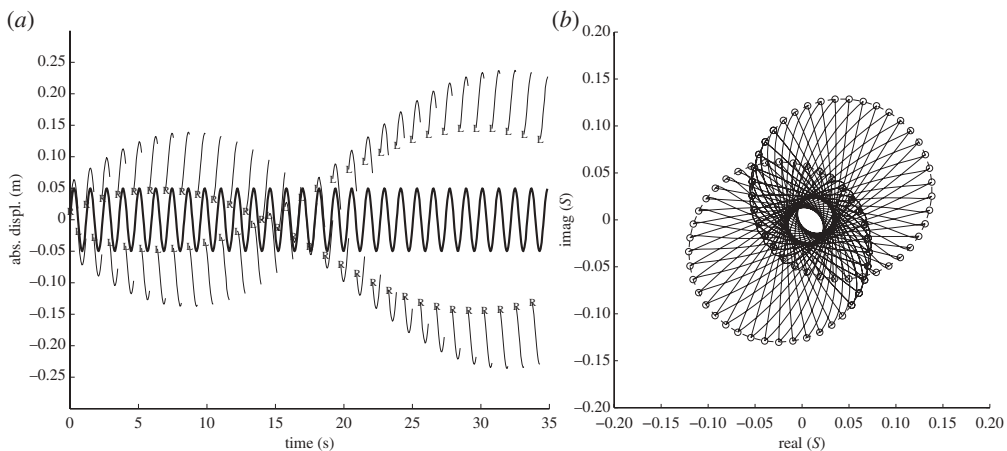


Figure 6. (a) The absolute foot placements of a detuned walker following Macdonald's model ($f_{br} = 0.839$ Hz and $f_{walk} = 0.86$ Hz), and (b) the corresponding quasi-periodic trajectory of the complex variable S .

where ω_w is the initial walking frequency, Ψ is the phase of the bridge motion and α is some constant angle offset. The coefficient C is a measure of the walker's susceptibility to synchronization, and X_{br} is the bridge amplitude. As the bridge amplitude grows, the evolution of the walker's phase θ is increasingly adjusted away from its original angular frequency ω_w by the sine term, this evolution depending on the relative phase $\Psi - \theta$ between bridge and walker.

Discretization is achieved by writing $\dot{\theta} = 2\pi/T_i$ and $\omega_w = 2\pi/T_0$, where T_0, T_i are the durations of the initial and the current walking cycle, respectively. Because T_i is evaluated at each footfall, the phase θ will be a constant at the point of evaluation (say 0 for a right foot and π for a left foot), and can be subsumed within the parameter α . The resulting candidate equation for the evolution of the pacing period is thus

$$T_i = T_0 - \frac{CX_{br}T_0^2}{2\pi} \sin(\Psi + \alpha), \quad (6.2)$$

where the final term has made the approximation that $T_i \approx T_0$.

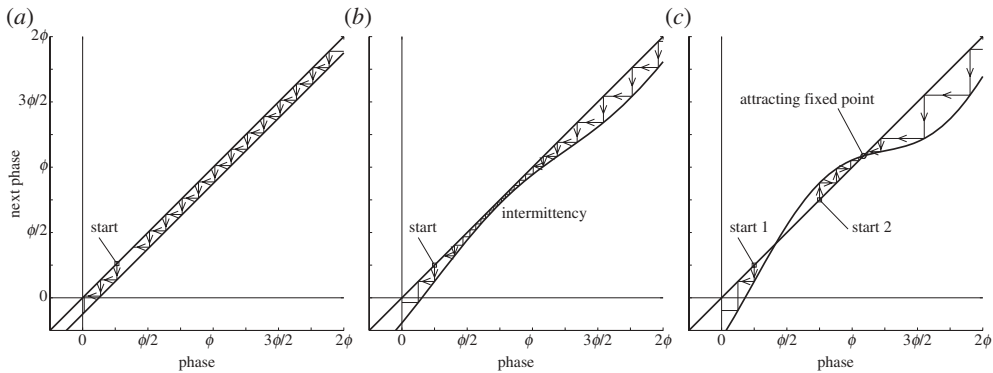


Figure 7. The evolution of walker phase for (a) zero, (b) small and (c) large bridge amplitudes. The walker/bridge frequency ratio is initially 1.07.

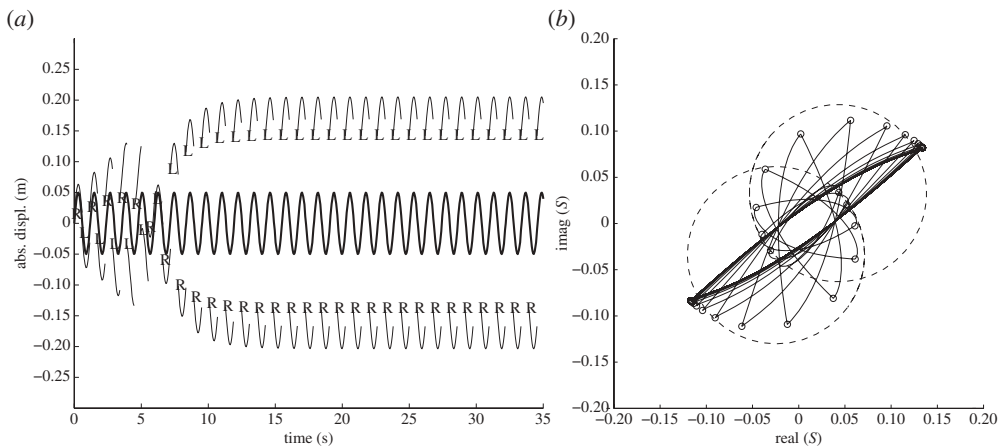


Figure 8. When timing adjustments are incorporated: (a) the absolute foot placements ($f_{br} = 0.839$ Hz and $f_{walk} = 0.86$ Hz) and (b) the trajectory of S converges to a nearby period-1 fixed point in synchrony with the bridge motions (cf. figure 6).

As an initial suggestion, we propose that the synchronization sensitivity parameter C be taken as $10 \text{ m}^{-1} \text{ s}^{-1}$, this being just over half the value suggested by Strogatz *et al.* [17]. The lower value is proposed here because just less than half of the $c_p = 300 \text{ N s m}^{-1}$ measured by Arup near 1 Hz is now generated by the flutter-like forces of the unsynchronized walkers.

The behaviour of this map for prescribed harmonic bridge motions (i.e. $\Psi = \omega t + \psi_0$) of zero, small and large amplitude is illustrated in figure 7. The walker/bridge frequency ratio is initially 1.07, and figure 7a corresponds to a stationary bridge, such that the frequency ratio remains fixed and the walker's phase slips by a constant angle relative to the bridge each cycle. For small bridge amplitudes (figure 7b), the degree of phase slipping varies each cycle, and there is intermittent behaviour when the walker's frequency becomes close to the bridge frequency for protracted periods. For larger bridge amplitudes (figure 7c), there are two fixed points, one of which is attracting, such that the walker's frequency converges to the bridge frequency and to a particular phase offset irrespective of the initial phase difference.

The effect of the small adjustments to the walking period on a walker following Macdonald's model is shown in figure 8. The previously quasi-periodic trajectory that involved prolonged foot-crossing evolves, converging to an uncrossed gait synchronized to the nearby frequency of the bridge.

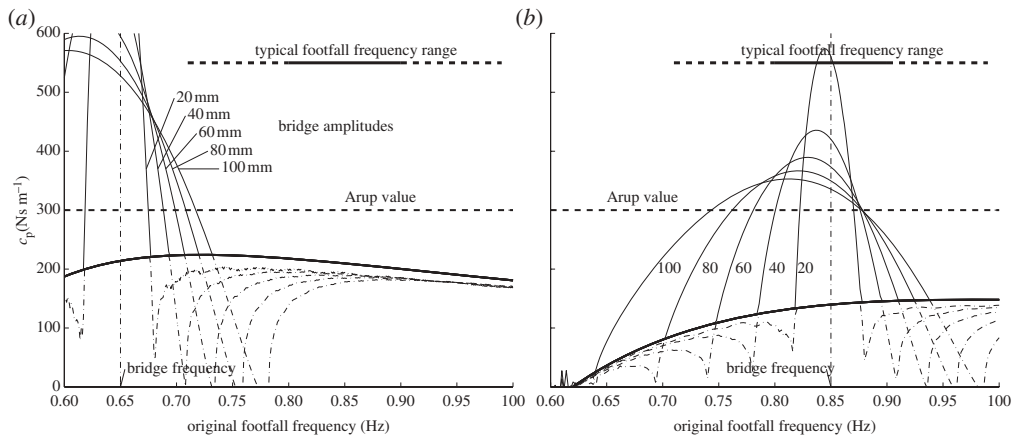


Figure 9. The c_p values for walkers with bridge frequencies of 0.65 Hz (a) and 0.85 Hz (b), with the timing adjustment of equation (6.2). The garlands of curves above the (solid) Macdonald curves are for bridge amplitudes of 20–100 mm.

For walkers who are not closely tuned to the bridge motion, the timing evolution equation will have little effect, and they will continue to walk at near their original pacing frequency, largely following the Macdonald model.

Figure 9 shows the effect of the footfall timing adjustment on final c_p values, plotted against original footfall frequency, for bridges oscillating at 0.65 Hz (figure 9a) and at 0.85 Hz (figure 9b). The Macdonald curves without synchrony (solid, bold) are shown. These correspond to a pedestrian mass of 74.4 kg, inverted pendulum frequency parameter $\Omega = \sqrt{g/L}$ with $L = 1.2$ m and $g = 9.81 \text{ m s}^{-2}$ and stability offset $b = 15.7$ mm. The control law is that based on absolute velocity. In each case, the Macdonald curve is garlanded by curves corresponding to walkers who synchronize to various bridge amplitudes in the range 0–100 mm, showing how previously detuned walkers become successively entrained as bridge amplitudes grow. For a 0.65 Hz bridge mode, few walkers are entrained, and the overall effective c_p —an average over the original footfall frequency distribution—would be close to the Macdonald values near 200 N s m^{-1} . Bridge frequencies near 0.85 Hz lie within the typical range of footfall frequencies, and here the Macdonald $c_p \approx 140 \text{ N s m}^{-1}$ values are augmented by synchronizing walkers, bringing the overall c_p closer to 300 N s m^{-1} . This combined model, then, is not too distant from the Arup values over the full 0.5–1 Hz range.

While this demonstrates how synchronization can lead to higher average c_p values, figure 9 shows that some walkers—those whose frequency offset is only just close enough to be significantly influenced by the synchronization mechanism—are entrained such that their final phases relative to the bridge lead to lower and even negative c_p values. These are shown dotted below the Macdonald curves in figure 9. How this arises can be understood from figure 7, in that the fixed point (where the sloping sine wave intersects the diagonal) shifts as the sine wave amplitude grows. The location of the fixed point is set by the phase constant α , which has been chosen to give large positive c_p for walkers who start near perfect tuning. The fixed point for walkers starting with a larger mistuning will be at a different phase, which will correspond to smaller and possibly negative c_p . In this model, mistuned walkers may even be entrained to walk indefinitely thereafter with crossed feet, which does not match the hypothesis that walkers will tend to select a comfortable gait.

To create a model wherein all walkers who synchronize do so to the same final phase, the x -coordinate of the fixed point of figure 7 must remain unchanged with respect to bridge amplitude and initial detuning. This can be achieved by setting

$$\alpha = \sin^{-1} \left(\frac{\Delta}{K} \right), \quad \text{with } \Delta = T_0 - T_{\text{br}} \quad \text{and} \quad K = \frac{CX_{\text{br}}T_0^2}{2\pi}. \quad (6.3)$$

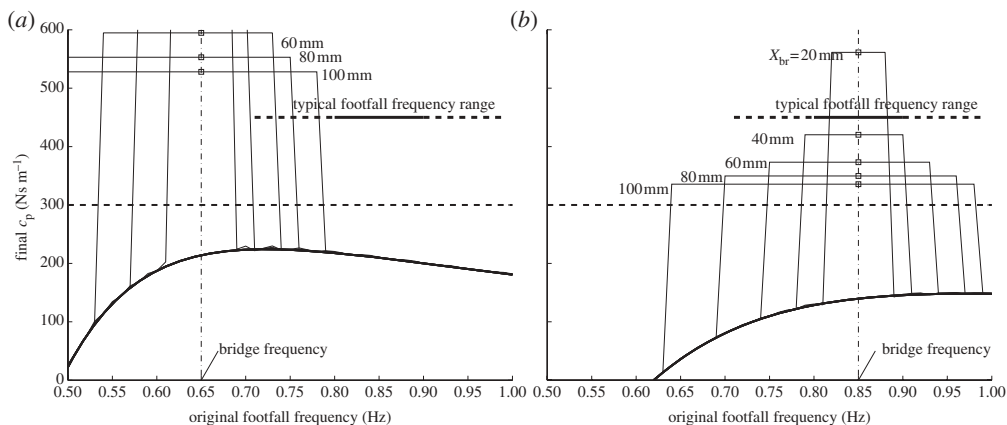


Figure 10. The c_p values for walkers on bridges having frequencies of 0.65 Hz (a) and 0.85 Hz (b), with the timing adjustment of equation (6.5) such that all walkers who synchronize do so to the same final phase of π relative to the bridge.

A candidate equation for the time $T_i/2$ to the next footfall is then given via

$$\frac{T_i}{2} = \frac{T_0}{2} \pm \frac{K}{2} \sin(\Psi + \alpha) \quad (6.4)$$

with the \pm corresponding to right or left footfalls. (A walker's phase θ is defined here to be zero at right footfall and π at left footfall, and the bridge phase $\Psi = \omega t + \Psi_0$ with $x = X_{br} \cos \Psi$ and $t = 0$ at the first right footfall.) This model leads all synchronizing walkers to a final phase of $\theta - \Psi = \pi$ relative to the bridge motions, corresponding to an uncrossed gait with feet well spaced, which would be reassuring to walkers who are concerned about their stability.

The above equations are only valid for $\Delta < K$ —that is, if the sine wave of figure 7 intersects the diagonal, such that a final fixed point exists. For detunings beyond this, we may choose to ignore the intermittent behaviour, and keep $T_i = T_0$ such that walkers simply obey the unadjusted Macdonald model unless amplitudes grow sufficiently to entrain them.

The resulting c_p values are shown in figure 10 for bridge frequencies of 0.65 and 0.85 Hz at various amplitudes. All entrained walkers converge to the same final relative phase and create the same final c_p for a given bridge frequency and amplitude. The height of each plateau is deducible from Macdonald's model applied to tuned walkers placing their footfalls at phase π relative to the bridge (with phases defined as above), giving

$$c_p = \frac{2m\Omega^2 A^2}{\pi\omega} (1 + e^{\Omega T/2}) \left(1 + \frac{b}{AX_{br}}\right), \quad (6.5)$$

where $A = 1/(1 + (\Omega/\omega)^2)$. The width of each plateau is determined by the synchronization parameter C of the Strogatz *et al.* model (taken here as $C = 10 \text{ m}^{-1} \text{ s}^{-1}$).

The rightmost halves of each diagram are of greatest interest, because these cover the typical walking frequencies of 0.75–1 Hz. For a 0.85 Hz bridge mode, unsynchronized Macdonald walkers provide c_p values of around 140 Ns m^{-1} , but synchronizing walkers can provide additional c_p , making plausible a total of around 300 Ns m^{-1} .

Describing the effects of a synchronized walker in terms of c_p values masks the simplicity of the forces they apply. At perfect tuning, the magnitude of the force in phase with the velocity is $c_p \omega X_{br}$, with c_p given by equation (6.5). Each synchronized walker could thus be represented as a tuned harmonic force with magnitude rising linearly from around 30 N on a static deck to around 180 N on a bridge undergoing large vibrations of around 100 mm amplitude. The magnitude of the total force felt by the bridge at the bridge frequency would thus rise super-linearly with amplitude as more walkers are entrained.

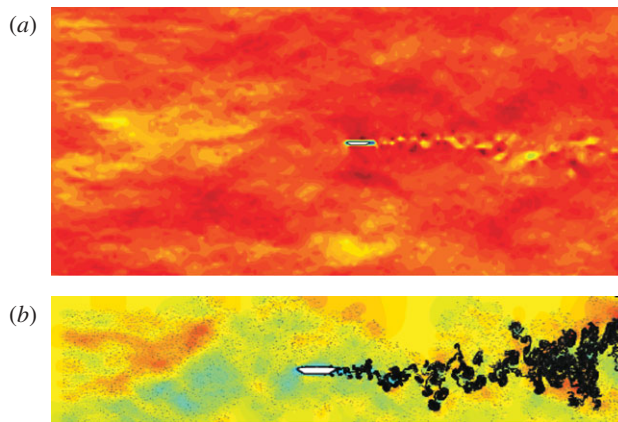


Figure 11. The flow around the Storebælt section using Prendergast's vortex particle formulation [42], showing how incident turbulence disrupts the regularity of the von Kármán street. Velocities and vortex particles are shown in (a) and (b) respectively. (Online version in colour.)

The exact description of how the pacing period evolves is of less importance than the fact that it can, and the foregoing synthesis of the Strogatz *et al.* and Macdonald models breaks down the previous demarcation between the two forcing mechanisms and shows how the two may interact to create the forces observed in the full-scale Arup experiments. For the designer, there may be less interest in the details of the biomechanics, given the simplicity of the Arup design recommendation of $c_p = 300 \text{ N s m}^{-1}$ for modes in the range 0.5–1 Hz. For many footbridges, the adoption of this value will mean that additional damping must be provided, perhaps in the form of tuned mass dampers. A complex mode formulation for addressing the complications that then arise from the localized damping is described in McRobie & Winslow [32].

7. The three-dimensional time domain case

In both the wind- and human-induced case, one can foresee a move towards total computation, whereby a designer creates a detailed three-dimensional finite-element model of the structure and immerses it in a computational wind tunnel or allows a virtual crowd to pass across it.

While fully three-dimensional computational fluid dynamic modelling is prevalent in aerospace and motor sport, the difference in scales for bridges—from spans of the order of kilometres down to boundary layer details requiring millimetre resolution to accurately capture the vorticity creation—is considerably more challenging. Even for aeronautical and automotive applications, full aeroelastic simulation is still in its infancy, often restricted to analysis of components.

The mesh-free nature of the vortex particle method lends itself well to analysis at differing scales and around moving structures. For example, Morgenthal's VXFLOW [24] provides high resolution in the boundary layers around moving surfaces, and achieves computational efficiency by discarding far-field resolution. However, extension to three dimensions is difficult, not only because of the large increase in the number N of particles whose N^2 interactions must be computed, but also because of three-dimensional complications such as vortex filament stretching. Such three-dimensional vortex models have been created [33] but their application to bridges remains distant.

In lieu of such fully three-dimensional models, the more computationally tractable analysis of parallel two-dimensional slices at sections along the deck has been proposed [34–40], with slices coupled via structural finite elements and via low-resolution interactions of the adjacent two-dimensional vorticity fields.

Although phenomenologically different from the fluid–structure instabilities, incident turbulence provides an additional complication. Prendergast & McRobie [41,42] show how the upstream release of appropriate vortex particles can create the desired horizontal and vertical turbulence spectra. Figure 11 shows how this not only causes buffeting, but also disrupts the regularity of the von Kármán street. The approach was extended by Rasmussen *et al.* [43] to calculate the along-wind and vertical aerodynamic admittances for static bridge decks. The method is restricted to static decks, there being little point in including incident turbulence in aeroelastic simulations, given that incident turbulence will be span-wise decorrelated. However, the possibility of analysing both turbulence and structural motion via parallel slices (as described above) remains.

For wind, then, the analysis of the whole-bridge three-dimensional fully coupled aeroelastic response with incident turbulence remains some years away, while the possibility of the parallel complete analysis for crowd-loading appears considerably closer.

The models of human walking discussed thus far, such as the majority of models for wind-structure interaction, are two dimensional. A model for the three-dimensional motion of pedestrians has been put forward by Morbiato *et al.* [44]. Here, an inverted pendulum model that can move laterally and longitudinally appears to be capable of producing the flutter-like force components. Moreover, it also predicts that a walker will—in certain frequency and amplitude ranges—synchronize to the bridge motions via a parametric interaction between lateral and longitudinal effects in regimes that form Arnol'd tongues across the parameter space. This elegance, though, comes at a cost of complexity.

A different form of three-dimensional model is described in Durupinar & Güdükbay [45], whose approach resembles that of video games and fire evacuation models wherein individual agents—represented graphically as virtual humanoids—respond to their local environments, avoiding obstacles and each other as they progress through the scene. This is perhaps the closest yet to fully three-dimensional discrete pedestrian modelling, and the prospect of designers walking virtual crowds across finite-element models of their bridges appears to be approaching. However, further experiments are required to refine not only the biomechanics of walking on a moving deck, but also the psychology of crowds, be they rush hour commuters or New Year's revellers. Such experiments not only can measure the induced forces but can use motion capture technology [46] to focus on the biomechanics. Such 'pedestrian imaging velocimetry'—applied to real crowds on real bridges—would appear to be the appropriate method of calibrating the computer humanoids.

Further three-dimensional effects concern the structure itself. If horizontal motions become large enough to cause a significant proportion of walkers to synchronize their footfalls near 1 Hz, then their vertical forces are also synchronized near 2 Hz and could dangerously excite a vertical mode in that vicinity. Moreover, there remains the possibility of parametric resonance between modes which are coupled by weak nonlinearities (as in the simple spring pendulum), such that energy fed into vertical modes may transfer to horizontal motion, and vice versa. Further yet, there are often modes—particularly on curved footbridges—which involve both horizontal and vertical responses at any point, meaning that vertical and horizontal effects cannot be so readily separated.

Somewhat paralleling turbulence in the fluid–structure case is inter- and intra-person variability. In time domain crowd models, individual balance control laws can be readily randomized. Based on the results of extensive laboratory experiments, Ingólfsson & Georgakis [47] proposed a stochastic load model wherein pedestrians exert forces at their walking frequency and also at the bridge frequency. Given the frequency and amplitude of the deck at each walker's present location, the c_p and $\rho_m m$ flutter derivatives are updated stochastically to match empirical statistical distributions. However, as has been argued, laboratory c_p values for single walkers might not be appropriate for crowds on a real bridge.

In summary, the parallels between fluid- and human-structure interaction exist into the more sophisticated three-dimensional analyses, with randomness manifesting itself as both buffeting and span-wise vortex decorrelation in the former, and as the variability of individuals in the

latter. Fully three-dimensional modelling in each case is in its nascent stages, with incident turbulence and three-dimensional vortex particle models in the aeroelastic case finding parallels in the agent-based ‘discrete pedestrian’ simulations in the human–structure case.

8. Differences

Although there are parallels between the two fields, there are differences. The primary difference concerns risk. The paper has thus far focused on modelling: given a scenario (a wind speed, a crowd), what is the bridge response? But there is also the question of which wind speed, which crowd. In wind engineering, there exist meteorological records from which extreme statistics can be drawn with some degree of confidence, and even possible climate non-stationarity can, in theory, be taken into account. In the human–structure case though, there are no systematic records, and designers are required to make assumptions about possibilities. The tendency to consider only well-behaved crowds, with perhaps some acknowledgement of small groups of vandals, ignores the extreme possibilities that have been observed. During millennial and similar celebrations, excited crowds can throng onto bridges, often with much involvement of alcohol; in December 2010, students were kettled to extreme densities on Westminster Bridge in London; there was a similar occurrence (albeit at lesser density) in October 2011 with the Occupy protesters on Brooklyn Bridge in New York; and in 2010 there was the Cambodian tragedy. Modelling walkers under normal conditions does not address such possibilities, and a systematic procedure for assessing the extremes of human–structure interaction is currently lacking. In the face of such uncertainty, resilience can be provided by the adoption of higher c_p values, leading to the prudent provision of more damping and more mass. In line with earlier sections, this paper asserts that the arguing down of c_p values based on theoretical models of normal walking or on the results of laboratory experiments on single walkers should be avoided.

9. Conclusions

The forces induced at the bridge frequency by walkers following Macdonald’s [19] model parallel those of flutter, while the synchronization model of Strogatz *et al.* [17] parallels vortex-induced lock-in. The recognition that flutter and vortex-induced vibration can interact led to the proposal that made minor adjustments to the Macdonald [19] model allowing walkers to lock-in. The resulting synthesis appears capable of explaining the high c_p values measured by the full-scale crowd load tests conducted by Arup over the full 0.5–1 Hz frequency range.

Further parallels were noted between the randomness inherent in wind engineering (incident turbulence or span-wise decorrelation of vortices shed) and the inter- and intra-personal variability inherent in human walking. Discretized models—vortex particle and discrete pedestrian—can be extended to incorporate such variability, but challenges remain. In wind engineering, the whole-bridge fully three-dimensional model with incident turbulence remains a formidable problem. In human–structure interaction the challenges in the comparable whole-bridge modelling of crowd loading lie more in developing a proper understanding of the biomechanics of walking on a moving structure and of the psychology of walking in various forms of crowd.

References

1. Farquharson FB *et al.* Aerodynamic stability of suspension bridges with special reference to the Tacoma Narrows Bridge, vol. I–V, 1949–1954. Bulletin 116, University of Washington Engineering Experimental Station, Seattle, WA.
2. Fujino Y, Pacheco B, Nakamura S, Warnitchai P. 1993 Synchronization of human walking observed during lateral vibration of a congested pedestrian bridge. *Earthq. Eng. Struct. Dyn.* **22**, 741–758. (doi:10.1002/eqe.4290220902).

3. Dallard P, Fitzpatrick A, Flint A, Low A, Ridsdill Smith R, Willford M, Roche M. 2001 London Millennium Bridge: pedestrian-induced lateral vibration. *Am. Soc. Civil Eng. J. Bridge Eng.* **6**, 412–417. (doi:10.1061/(ASCE)1084-0702(2001)6:6(412))
4. Venuti F, Bruno L. 2009 Crowd-structure interaction in lively footbridges under synchronous lateral excitation: a literature review. *Phys. Life Rev.* **6**, 176–206. (doi:10.1016/j.plev.2009.07.001)
5. Anon. 2010 Swaying causes running wariness over Bosphorus Bridge. *Hürriyet Daily News*, 18 October 2010. See <http://www.hurriyetdailynews.com/default.aspx?pageid=438&n=swinging-bosporus-bridge-alerts-experts-2010-10-18>.
6. Anon. 2010 Cambodia stampede: swaying bridge blamed for panic. *The Guardian*, 24 November 2010. See <http://www.guardian.co.uk/world/2010/nov/24/cambodia-stampede-swaying-bridge>.
7. Bachmann H, Ammann W. 1987 *Vibrations in structures: induced by man and machines*. Zurich, Switzerland: International Association for Bridge and Structural Engineering.
8. Fletcher MS, Parker JS. 2003 Dynamics of the Hungerford Millennium footbridges, UK. *Proc. ICE Bridge Eng.* **156**, 57–62. (doi:10.1680/bren.2003.156.2.57)
9. Black M, Webster G. 2006 Jane Coston cycle bridge: a model for managing vibration. *Proc. ICE Civil Eng.* **159**, 120–125.
10. Davenport AG. 1961 A statistical approach to the treatment of wind loading on tall masts and suspension bridges. PhD thesis, Department of Civil Engineering, University of Bristol, UK.
11. Engineering Science Data Unit. 2012 Wind Engineering Series. IHS ESDU, London, UK. See http://www.esdu.com/cgi-bin/ps.pl?sess=unlicensed_1130410230221clt&t=ser&p=ser_wind.
12. Lawson T. 2001 *Building aerodynamics*. London, UK: Imperial College Press.
13. Dyrbye C, Hansen SO. 1997 *Wind loads on structures*. London, UK: Wiley.
14. Feng CC. 1968 The measurement of vortex-induced effects in flow past stationary and oscillating circular and d-section cylinders. Master's thesis, Department of Mechanical Engineering, University of British Columbia, Canada.
15. Larsen A, Eisdahl S, Andersen JE, Vejrum T. 2000 Storebælt suspension bridge: vortex shedding excitation and mitigation by guide vanes. *J. Wind Eng. Ind. Aerodyn.* **88**, 283–296. (doi:10.1016/S0167-6105(00)00054-4)
16. McRobie FA, Morgenthal G. 2002 Full-scale section model tests on human–structure lock-in. In *Proc. 1st Int. Conf. on the Design and Dynamic Behaviour of Footbridges, Paris, France, 20–22 November 2002*. Paris, France: Association Francaise de Genie Civil and Office Technique pour l'Utilisation de l'Acier.
17. Strogatz SH, Abrams DM, McRobie A, Eckhardt B, Ott E. 2005 Crowd synchrony on the Millennium Bridge. *Nature* **438**, 43–44. (doi:10.1038/438043a)
18. Barker C. 2002 Some observations on the nature of the mechanism that drives the self-excited lateral response of footbridges. In *Proc. 1st Int. Conf. on the Design and Dynamic Behaviour of Footbridges, Paris, France, 20–22 November 2002*. Paris, France: Association Francaise de Genie Civil and Office Technique pour l'Utilisation de l'Acier.
19. Macdonald JHG. 2009 Lateral excitation of bridges by balancing pedestrians. *Proc. R. Soc. A* **465**, 1055–1073. (doi:10.1098/rspa.2008.0367)
20. Theodorsen T. 1934 General theory of aerodynamic instability and the mechanism of flutter. Technical Report 496, National Advisory Committee for Aeronautics, Washington, DC.
21. Scanlan RH, Tomko J. 1971 Airfoil and bridge deck flutter derivatives. *J. Eng. Mech. Div. ASCE* **97**, 1717–1737.
22. Bocian M, Macdonald JHG, Burn JF. 2012 Biomechanically inspired modelling of pedestrian-induced forces on laterally oscillating structures. *J. Sound Vib.* **331**, 3914–3929. (doi:10.1016/j.jsv.2012.03.023)
23. Ingólfsson ET, Georgakis CT, Ricciardelli F, Jonsson J. 2011 Experimental identification of pedestrian-induced lateral forces on footbridges. *J. Sound Vib.* **330**, 1265–1284. (doi:10.1016/j.jsv.2010.09.034)
24. Morgenthal G. 2002 Aerodynamic analysis of structures using high-resolution vortex particle methods. PhD thesis, University of Cambridge, UK.
25. Deniz S, Staubli T. 1997 Oscillating rectangular and octagonal profiles: interaction of leading and trailing edge vortex formation. *J. Fluids Struct.* **11**, 3–31. (doi:10.1006/jfls.1996.0065)
26. Deniz S, Staubli T. 1998 Oscillating rectangular and octagonal profiles: modelling of fluid forces. *J. Fluids Struct.* **12**, 859–882. (doi:10.1006/jfls.1998.0171)

27. Simiu E, Scanlan RH. 1996 *Wind effects on structures*. London, UK: Wiley.
28. Ehsan F, Scanlan RH. 1988 Vortex-induced vibration of flexible bridges. *J. Eng. Mech. Div. ASCE* **116**, 1392–1411. (doi:10.1061/(ASCE)0733-9399(1990)116:6(1392))
29. Scanlan RH. 1998 Bridge flutter derivatives at vortex lock-in. *J. Struct. Eng.* **124**, 450–458. (doi:10.1061/(ASCE)0733-9445(1998)124:4(450))
30. Billah K, Scanlan R. 1991 Resonance, Tacoma Narrows Bridge failure, and undergraduate physics textbooks. *Am. J. Phys.* **59**, 118–124. (doi:10.1119/1.16590)
31. Larsen A. 2000 Aerodynamics of the Tacoma Narrows Bridge: 60 years later. *Struct. Eng. Int.* **4**, 243–248. (doi:10.2749/101686600780481356)
32. McRobie FA, Winslow P. 2012 The lateral dynamic stability of Stockton Infinity Footbridge using complex modes. *Struct. Eng. Int.* **4**, 545–551. (doi:10.2749/101686612X13363929518108)
33. Walther JH, Koumoutsakos P. 2001 Three-dimensional vortex methods for particle-laden flows with two-way coupling. *J. Comput. Phys.* **167**, 39–71. (doi:10.1006/jcph.2000.6656)
34. Pesmajoglou S, Graham JMR. 1993 Prediction of yaw loads on a horizontal axis wind turbine. In *Proc. ECWEC (European Community Wind Energy Conference), Lübeck-Travemünde, Germany, 8–12 March 1993*. Brussels, Belgium: European Wind Energy Association.
35. Giannakidis G, Graham JMR. 1997 Prediction of loading on a HAWT rotor including effects of stall. In *Proc. European Wind Energy Conference, Dublin, Ireland, 6–9 October 1997* (ed. R Watson). Brussels, Belgium: European Wind Energy Association.
36. Morgenthal G, McRobie FA. 2002 A comparative study of numerical methods for fluid–structure interaction in long-span bridge design. *J. Wind Struct.* **5**, 101–114.
37. Willden RHJ, Graham JMR. 2004 Multi-modal vortex-induced vibrations of a vertical riser pipe subject to a uniform current profile. *Eur. J. Mech. Fluids B* **23**, 209–218. (doi:10.1016/j.euromechflu.2003.09.011)
38. Willden RHJ, Graham JMR. 2001 Numerical prediction of VIV on long flexible circular cylinders. *J. Fluids Struct.* **15**, 659–669. (doi:10.1006/jfls.2000.0359)
39. Flatschart R, Meneghini J, Saltara F, Lima A, Gioria R. 2005 Parallel simulations of flow around high aspect ratio cylinders employing MPI. In *Proc. Mecánica Computacional, Buenos Aires, Argentina, 16–18 November 2005* (ed. A Larreteguy), vol. XXIV, pp. 1795–1804. Santa Fe, Argentina: Asociacion Argentina de Mecanica Computacional.
40. Le Cunff C, Biolley F, Fontaine E, Etienne S, Facchinetti M. 2002 Vortex-induced vibrations of risers: theoretical, numerical and experimental investigation. *Oil Gas Sci. Technol.* **57**, 59–69. (doi:10.2516/ogst:2002004)
41. Prendergast JM, McRobie FA. 2006 Simulation of 2D unsteady wind by a vortex method and application to studying bluff body flow. In *Proc. 7th UK Conf. on Wind Engineering, Glasgow, UK, 4–6 September 2006*, pp. 1–4. London, UK: Wind Engineering Society.
42. Prendergast JM. 2007 Simulation of unsteady 2-D wind by a vortex method. PhD thesis, University of Cambridge, UK.
43. Rasmussen JT, Hejlesen MM, Larsen A, Walther JH. 2010 Discrete vortex method simulations of the aerodynamic admittance in bridge aerodynamics. *J. Wind Eng. Ind. Aerodyn.* **98**, 754–766. (doi:10.1016/j.jweia.2010.06.011)
44. Morbiato T, Vitaliani R, Saetta A. 2011 Numerical analysis of a synchronization phenomenon: pedestrian–structure interaction. *Comp. Struct.* **89**, 1649–1663. (doi:10.1016/j.compstruc.2011.04.013)
45. Durupinar F, Güdükbay U. 2010 Visualization of crowd synchronization on footbridges. *J. Vis.* **13**, 69–77. (doi:10.1007/s12650-009-0012-7)
46. McRobie A, Morgenthal G, Lasenby J, Ringer M. 2003 Section model tests on human–structure lock-in. *Proc. Inst. Civil Eng. Bridge Eng.* **156**, 71–79. (doi:10.1680/bren.2003.156.2.71)
47. Ingólfsson ET, Georgakis CT. 2011 A stochastic load model for pedestrian-induced lateral forces on footbridges. *Eng. Struct.* **33**, 3454–3470. (doi:10.1016/j.engstruct.2011.07.009)